Peeling-Stiffening Self-Adhesive Ionogel with Superhigh Interfacial Toughness

Yingkun Shi, Baohu Wu, Shengtong Sun,* and Peiyi Wu*

Self-adhesive materials that can directly adhere to diverse solid surfaces are indispensable in modern life and technologies. However, it remains a challenge to develop self-adhesive materials with strong adhesion while maintaining its intrinsic softness for efficient tackiness. Here, a peeling-stiffening self-adhesive ionogel that reconciles the seemingly contradictory properties of softness and strong adhesion is reported. The ionogel contains two ionophilic repeating units with distinct associating affinities, which allows to adaptively wet rough surface in the soft dissipating state for adhering, and to dramatically stiffen to the glassy state upon peeling. The corresponding modulus increases by 117 times driven by strain-rate-induced phase separation, which greatly suppresses crack propagation and results in a super high interfacial toughness of 8046 $\mid m^{-2}$. The self-adhesive ionogel is also transparent, self-healable, recyclable, and can be easily removed by simple moisture treatment. This strategy provides a new way to design high-performance self-adhesive materials for intelligent soft devices.

1. Introduction

Adhesive materials that stick on diverse solid surfaces are essential for a variety of applications, including stickers, sealants, implantable devices, soft electronics, soft robotics, and microfluidics. Despite strong van der Waals attractions at the molecular scale that can produce forces per unit area orders of magnitude larger than atmospheric pressure, macroscopic objects hardly adhere. This is known as the "adhesion paradox," which arises from the surface roughness that is present in all solids at different length scales. The adhesion strength generally decays rapidly as the surface roughness increases,

Y. Shi, S. Sun, P. Wu

State Key Laboratory for Modification of Chemical Fibers and Polymer Materials

College of Chemistry and Chemical Engineering and Center for Advanced Low-dimension Materials

Donghua University

2999 North Renmin Road, Shanghai 201620, China

E-mail: shengtongsun@dhu.edu.cn; wupeiyi@dhu.edu.cn

B. Wu

Jülich Centre for Neutron Science (JCNS) at Heinz Maier-Leibnitz Zentrum (MLZ) Forschungszentrum Jülich

Lichtenbergstr. 1, 85748 Garching, Germany

reducing the contact area for adhesion.^[6] To overcome the adhesion paradox, high adhesion strength is usually achieved by chemically or physically curing a liquid precursor for sufficient surface wetting.^[4,7–13] However, the external stimuli applied for curing, such as heat, solvent evaporation, and UV irradiation, are both laborious and energy-intensive, and the resultant adhesion is often difficult to remove for extended reuse.

Self-adhesive materials represent another important strategy for overcoming the adhesion paradox. They stick on almost any solid surface by simply applying a normal pressure. To wet the rough surface, the effective moduli of self-adhesive materials must be designed to be lower than 0.3 MPa, as captured by the Dahlquist criterion for efficient tackiness. [14,15] Following this principle, researchers have developed a variety of gecko-inspired self-adhesive hairy pads and pressure-sensitive

adhesives.^[16-20] However, despite their ease to use and ondemand debonding, current self-adhesive materials still have weak adhesion with a relatively low interfacial toughness (generally <2000 J m⁻²) compared to cured adhesive materials. This is mainly due to the weakened fracture tolerance of self-adhesive materials upon peeling, which is limited by the desired softness for surface tackiness. To overcome the seemingly contradictory properties of intrinsic softness and strong adhesion, researchers have proposed a few remedial solutions involving catechol chemistry,^[21] electrochemistry,^[22,23] structural toughening,^[24-26] surface modification,^[27] nanoparticle/interlayer glues,^[28,29] and topological cross-linking.^[30] Nonetheless, the resulting adhesion strengths are still not as satisfactory as those of cured adhesive materials, and the extra treatment may also pose additional energy costs and unwanted permanent adhesion.

We notice that self-adhesive materials generally adhere and peel at different strain rates or frequencies (0.01–1 Hz for adhering and 10–100 Hz for peeling). This frequency response also constitutes the rheological basis for designing high-performance pressure-sensitive adhesives with maximum tackiness close to the gel point (where the elastic and viscous moduli are approximately equal, $G' \approx G''$) and easy peeling in the rubbery state (G' > G'') (**Figure 1a**). [15,31] Therefore, we anticipate that if self-adhesive materials work in the sharp dissipating-to-glassy transition range, the good surface wettability upon adhering in the soft dissipating state (liquid-like, G' < G'') and strong adhesion upon peeling in the stiffened glassy state (solid-like, G' > G'')

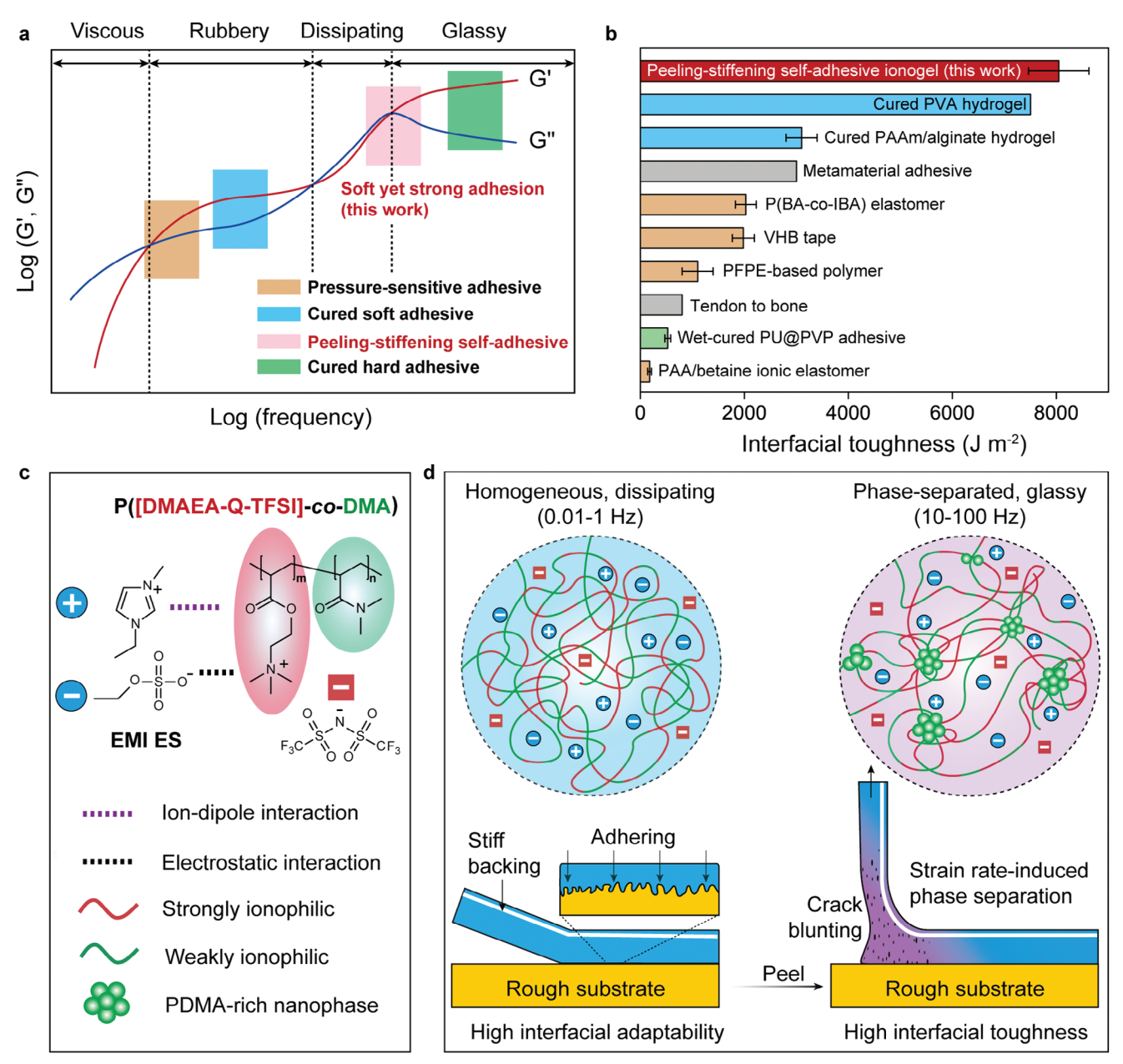


Figure 1. a) Typical rheology of viscoelastic polymers. Conventional adhesive materials are generally designed to work in either the viscous-to-rubbery (pressure-sensitive adhesive), rubbery (cured soft adhesive), or glassy (cured hard adhesive) regions. By contrast, the present peeling–stiffening self-adhesive materials work in the dissipating-to-glassy transition region, which reconciles the trade-off between intrinsic softness (adhering at low frequencies) and strong adhesion (peeling–stiffening at high frequencies). b) Comparison of the interfacial toughness of the present peeling–stiffening self-adhesive ionogel with other representative adhesive materials (data in Table S1 in the Supporting Information). c) Chemical structure of the peeling–stiffening self-adhesive ionogel. In the designed copolymer ionogel, P[DMAEA-Q-TFSI] moieties are more ionophilic than PDMA. d) Schematic working mechanism. Upon adhering at low frequencies, the ionogel is homogeneous in the liquid-like dissipating state, allowing for high interfacial adaptability. Upon peeling at higher frequencies, strain-rate-induced phase separation of PDMA moieties takes place, forcing the peeled area into a highly stiffened glassy state. The stiffness increase and nanophase-enhanced crack tolerance simultaneously contribute to a superhigh interfacial toughness.

may be well reconciled. Such a peeling–stiffening behavior of self-adhesive materials is expected to take full advantage of surface roughness for mechanical interlocking without recalling the curing mechanism for strong adhesion. Moreover, the peeling–stiffening response may be further sharpened by adopting a supramolecular material design, which is known to be strongly rate-dependent.^[32]

Based on the above hypothesis, in this work, we report the first example of a peeling–stiffening self-adhesive ionogel with an unprecedented high interfacial toughness, surpassing nearly all reported adhesive materials (see comparison in Figure 1b and Table S1 in the Supporting Information). The supramolecular ionogel was particularly designed from an associating copolymer, P([DMAEA-Q-TFSI]-co-DMA)

(DMAEA-Q-TFSI: 2-acryloyloxyethyl trimethylammobis(trifluoromethylsulfonyl)imide; DMA: N,Ndimethylacrylamide). Both the P[DMAEA-O-TFSI] and PDMA moieties are compatible with the same ionic liquid (i.e., ionophilic), 1-ethyl-3-methylimidazolium ethyl sulfate (EMI ES), but have distinct associating affinities (P[DMAEA-Q-TFSI] is more ionophilic than PDMA) (Figure 1c). By carefully optimizing the recipe and internal interactions, the as-obtained ionogel is initially soft and homogeneous at the liquid-like dissipating state $(G' \approx 0.29 \text{ MPa}, \text{ the loss factor } \tan \delta = G''/G' = 2.1 \text{ at } 0.01 \text{ Hz}),$ which can easily adhere to any rough substrates with high interfacial adaptability (Figure 1d). However, upon peeling at higher frequencies, the dynamic phase separation of PDMA moieties takes place along the strain direction, forcing the peeled area into a highly stiffened glassy state ($G' \approx 34.2$ MPa at 100 Hz). Such strain-rate-induced phase separation greatly suppresses crack propagation at the interface and boosts the interfacial toughness to a superhigh value (8046 \pm 582 J m⁻² on a typical rough glass substrate). Furthermore, the supramolecular ionogel also features a few other fascinating properties, such as high stretchability (764%), high transparency (≈98%), self-healing (≈96% efficiency), full recyclability, and on-demand debonding (bonding/debonding ratio = 59). We finally demonstrated the application of the self-adhesive ionogel in smart laminated glass for simultaneous impact protection and electrical sensing.

2. Results and Discussion

2.1. Synthesis and Optimization of Self-Adhesive Ionogel

The peeling-stiffening self-adhesive ionogel was prepared by one-step UV-induced radical copolymerization of DMAEA-Q-TFSI and DMA in the presence of EMI ES. The molar ratio of DMAEA-Q-TFSI to DMA was fixed to 1:1 with optimized mechanical properties (Figure S1, Supporting Information), and only the mass content of EMI ES was adjusted relative to the total monomer. In this material, P[DMAEA-Q-TFSI] is expected to be more compatible with EMI ES than PDMA owing to its ionic structure. We confirmed this by comparing the glass transition temperatures (T_{σ}) of their homopolymer and copolymer ionogels with different EMI ES contents. As shown in Figure 2a and Figure S2 (Supporting Information), the T_as of P[DMAEA-Q-TFSI], PDMA, and their copolymer ionogels all decreased with increasing EMI ES contents, suggesting that EMI ES can plasticize both the P[DMAEA-Q-TFSI] and PDMA moieties. Notably, the faster decrease in T_{σ} for P[DMAEA-Q-TFSI]/EMI ES reveals a more noticeable plasticizing effect, which also corresponds to a lower apparent activation energy (E_a) for the same content of EMI ES (Figure 2b; see calculation details in Figures S3-S5 in the Supporting Information). The plasticizing effect of EMI ES on the copolymer and the corresponding E_a are just intermediate between those of their homopolymers, suggesting that DMAEA-Q-TFSI and DMA were homogeneously copolymerized in the ionogel without apparent phase separation. Therefore, the mechanical and rheological properties of the copolymer ionogel can be finely tuned by simply adjusting EMI ES content.

Owing to their homogeneous structure, all the copolymer ionogels with varied EMI ES contents (0–30 wt%) are optically transparent with an ultrahigh transmittance of \approx 98% in the visi-

ble range (Figure 2c). However, the mechanical properties of the ionogels are strongly affected by EMI ES content. As the EMI ES content increased, the ionogel became softer and more ductile (Figure 2d), in line with the changes in glass transition temperatures. As calculated by the single-edge notch tension method, a maximum fracture energy of 34.6 kJ m⁻² was achieved at the EMI ES content of 15 wt% (Figure 2e and Figure S6 (Supporting Information)), a key parameter for evaluating fracture-related adhesion behavior.[7,10,33] The calculated fractocohesive length or dissipation zone size at this composition was ≈2 mm, below which the ultimate mechanical properties are almost independent of crack length.[34] Notably, the composition of 15 wt% corresponds to a glass transition temperature of 23 °C, very close to room temperature. This finding is not surprising, since the glass transition (or dissipating) state has high interchain friction and energy dissipation, which are favorable for improving fracture-related mechanical properties. [35-37] The fracture strength and elongation of the ionogel at the EMI ES content of 15 wt% were 4.3 MPa and 764%, respectively, making the material strong enough to lift a 2 kg weight load (8000 times its own weight) (inset in Figure 2d). The critical EMI ES content of 15 wt% was also supported by low-field 19F NMR spectra, in which the activity of TFSI from the copolymer increased rapidly with increasing EMI ES content from 0 to 15 wt%, but reached a plateau from 15 to 30 wt% (Figure \$7, Supporting Information).

To investigate the rheological state of the copolymer ionogel with varying EMI ES contents at room temperature (25 °C), we performed time-mass fraction superposition on their respective rheological data using the content of 15 wt% as the reference (Figure 2f; see original data in Figure S8 in the Supporting Information; the 0 wt% sample without ionic liquid was too brittle to obtain reliable data). Apparently, with increasing EMI ES contents, the ionogel gradually transitioned from the glassy state (10 wt%) to the dissipating state (15-20 wt%) and finally to the rubbery state (25–30 wt%). The $\tan\delta$ value at the frequency of 0.01 Hz (typical for pressure-sensitive adhesives to evaluate tackiness)^[15] was used as the primary indicator of the initial quasistatic state. As shown in Figure 2g, the ionogels with the EMI ES contents of 10, 25, and 30 wt% had $tan\delta$ values lower than 1, corresponding to a solid-like property in the glassy and rubbery states. By contrast, the $\tan\delta$ values of the ionogels with the EMI ES contents of 15 and 20 wt% are much higher than 1 ($tan\delta = 2.1$ at 15 wt%), corresponding to a liquid-like property in the dissipating state. As illustrated in Figure 1d, the liquid nature of the ionogel can greatly facilitate interfacial adaptability to overcome the classical adhesion paradox of self-adhesive materials.

We further measured the adhesive interfacial toughnesses of the copolymer ionogels with the standard 90° peeling method using a woven cotton fabric as the stiff backing (see schematic sample preparation in Figure S9 in the Supporting Information) and ground glass as the representative rough substrate (average roughness $R_a \approx 457$ nm, Figure S10, Supporting Information). After pressing the ionogel on the rough glass substrate and holding for 24 h, superhigh interfacial toughnesses can be obtained upon peeling (Figure 2h,i). A maximum interfacial toughness of 8046 ± 582 J m⁻² was observed at the EMI ES content of 15 wt% (see reproducible data in Figure S11 in the Supporting Information). This value far exceeds nearly all the reported cured or self-adhesive materials to the best of our knowledge (Figure 1b

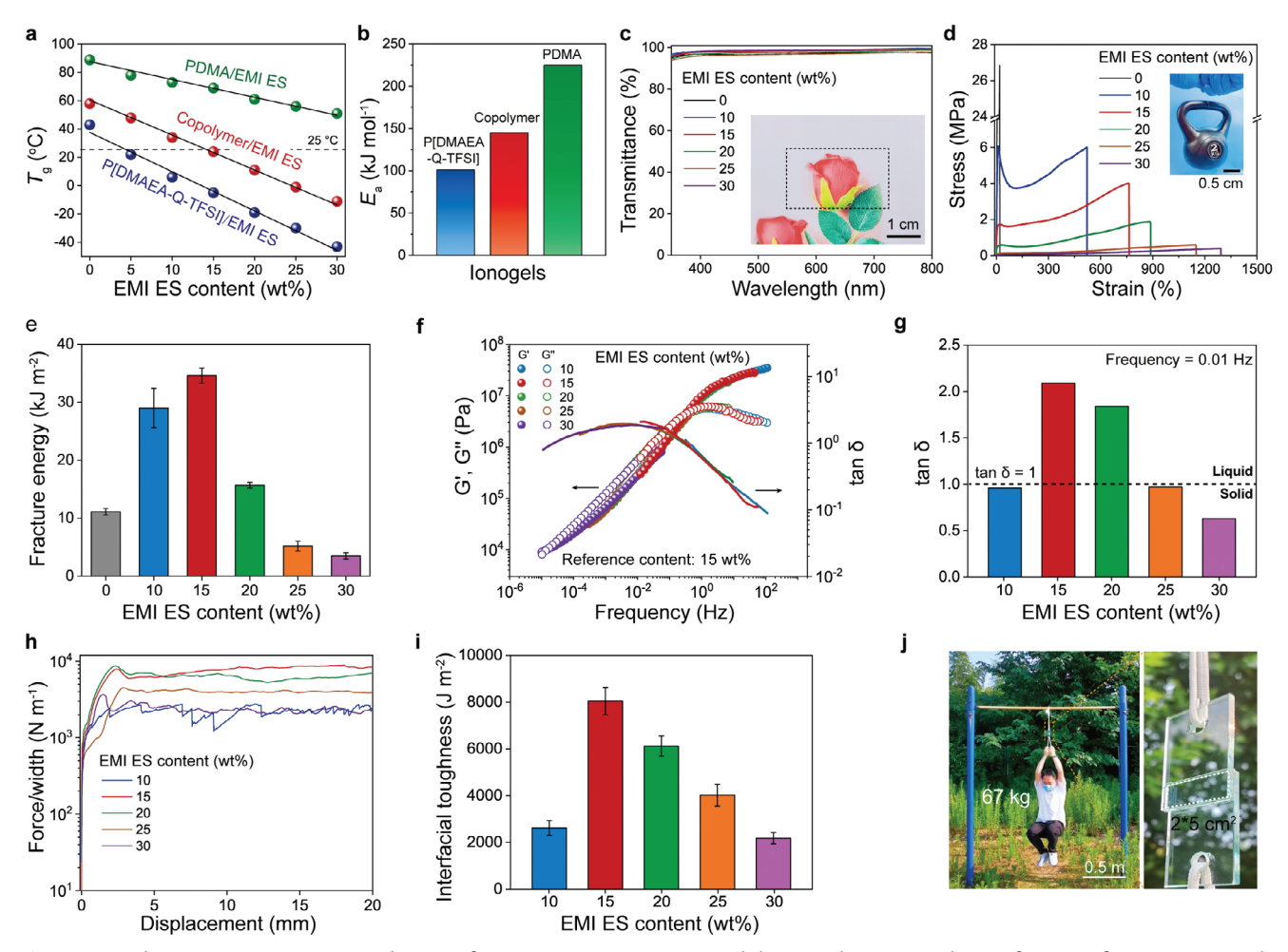


Figure 2. a) Glass transition temperature changes of PDMA, P[DMAEA-Q-TFSI], and their copolymer ionogels as a function of EMI ES content. b) Comparison of the apparent activation energies of the three samples at an EMI ES content of 15 wt%. c) Transmittance curves of the copolymer ionogels with varying EMI ES contents (film thickness = 0.3 mm; the inset shows a photo of the ionogel with 15 wt% EMI ES). d) Tensile stress–strain curves (strain rate = 0.1 s⁻¹; the inset shows a photo of a 0.25 g weight ionogel with 15 wt% EMI ES lifting a 2 kg weight load). e) The corresponding fracture energies. f) Time–mass content superposition rheological master curve of the ionogel at the reference content of 15 wt% (T = 25 °C). g) EMI ES-content-dependent tanδ values measured at 0.01 Hz. h,i) 90° peeling force–displacement curves and the corresponding interfacial toughnesses of the ionogels adhered to a rough glass substrate (peeling speed: 50 mm min⁻¹). j) The two glasses adhered by self-adhesive ionogel can sustain a 67 kg adult. The error bars represent ±standard deviation (SD) from the mean value (n = 3).

and Table S1 (Supporting Information); see comparison data with commercial VHB, Kapton, and double-sided tapes in Figure S12 in the Supporting Information). Notably, this trend is fully consistent with the results of $\tan\delta$ values and fracture energies, suggesting that interfacial adaptability and fracture tolerance are the two key factors for achieving strong adhesion. Indeed, the interfacial failure of the ionogel during peeling was always accompanied by its cohesive fracture, resulting in tearing stripes (Movie S1, Supporting Information).

All the above measurements pointed to an optimal EMI ES content of 15 wt%, with the desired dissipating-to-glassy transition upon peeling and the highest interfacial toughness. Unless otherwise stated, all the ionogels mentioned hereafter have this content. We further carried out the peeling tests of this ionogel on other rough substrates, such as iron, copper, aluminum, pottery, wood, and plastic, and obtained considerably high interfacial toughnesses (4590–6888 J m⁻², Figure S13, Sup-

porting Information), demonstrating the universal strong adhesion of this ionogel. Notably, the abundant physical attractions between the ionogel and the substrates should also contribute to the observed high interfacial toughnesses (Figure S14, Supporting Information), which may help with the stress transfer from interfacial debonding to bulk tearing. To further demonstrate the strong adhesion of the ionogel, we also adhered two glasses with a 2×5 cm² ionogel, which sustained a 67 kg adult (Figure 2j and Movie S2 (Supporting Information); measured lapshear strength ≈ 1.7 MPa, Figure S15, Supporting Information).

2.2. Interfacial Adaptability and Peeling-Stiffening Response

As mentioned above, the rheological liquid-like dissipating behavior of the self-adhesive ionogel at the quasistatic state leads to excellent interfacial adaptability upon adhering. To illustrate

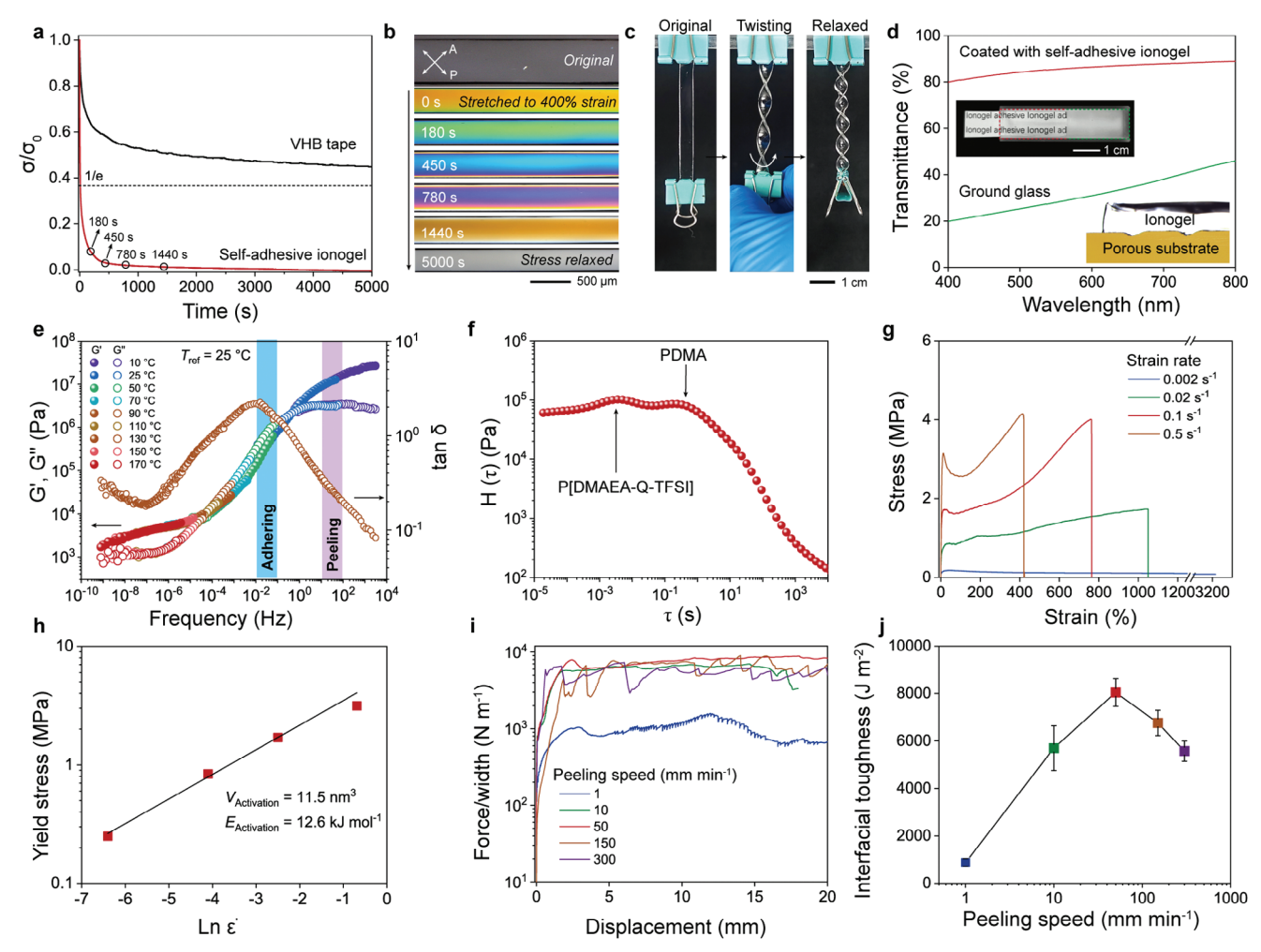


Figure 3. a) Stress relaxation curves of the self-adhesive ionogel (EMI ES content = 15 wt%) and commercial VHB tape measured at 400% tensile strain. b) Time-dependent polarized optical microscopy images of the ionogel during stress relaxation. c) The ionogel film can be programmed into a twisted shape with full stress relaxation. d) Photos and transmittance curves of ground glasses with/without self-adhesive ionogel. e) Time-temperature superposition rheological and $\tan \delta$ curves of the ionogel at the reference temperature of 25 °C. f) Relaxation time spectrum determined via the iterative fitting of the master curve. g) Tensile curves of the ionogel at different strain rates. h) Linear fitting of yield stresses as a function of the natural logarithm of strain rates (ϵ). i,j) Measured peeling forces per width and the corresponding interfacial toughnesses of the ionogel adhered to a ground glass at different peeling speeds. The error bars represent ±SD from the mean value (n = 3).

this property, we first performed stress relaxation tests on the ionogel, which can directly reflect its shape-shifting ability. As shown in Figure 3a, when the ionogel was stretched to 400% strain, the generated stress rapidly relaxed with a very short relaxation time of 14 s. The stress could be completely eliminated in 5000 s, demonstrating the occurrence of full stress relaxation. By contrast, commercial pressure-sensitive adhesive like VHB tape was elastic with a relaxation time much longer than 5000 s. The evolution process of stress relaxation was also monitored by the interference color changes under polarized light observation (Figure 3b). Over time, the stress-induced interference color gradually changed from yellow to green, blue, purple, brown, and finally faded in 5000 s, demonstrating the time-dependent full stress relaxation.[38] As a result, if we twisted an ionogel film and held it for 120 min, the ionogel could obtain a new permanent shape (Figure 3c and Movie S3 (Supporting Information)). Under adhesion scenarios, when we pressed the ionogel on a

ground glass, the ionogel would gradually flow and fill the surface gaps and bumps, greatly enhancing the glass's transparency from $\approx 30\%$ to $\approx 85\%$ (Figure 3d).

To comprehensively investigate the frequency-dependent rheological behavior of the self-adhesive ionogel, we plotted its time–temperature superposition master curve at a reference temperature of 25 °C (Figure 3e; see temperature-dependent vertical shift factors in Figure S16 in the Supporting Information). The ionogel exhibited mainly three distinct regions (i.e., rubbery, dissipating, and glassy) at the measured temperatures. The ionogel's whole chain reptation time ($\tau_{\rm rep}$) calculated from the reciprocal of the critical frequency between the viscous and rubbery regions, exceeds 10^9 s, which is extremely long for resisting creep under storage. [35] Between 0.01 and 100 Hz, which covers the adhering and peeling events, the ionogel clearly spans both the dissipating and glassy regions. The $\tan\delta$ values higher than 1 in the dissipating region again validate the liquid nature of the ionogel at the

quasistatic state. The Kuhn segment relaxation time (τ_0) calculated from the reciprocal of the crossover frequency between the dissipating and glassy regions (\approx 0.43 Hz) is 2.3 s, which is on the experimental timescale to enable peeling-induced chain freezing and macroscopic stiffening.

Upon increasing the frequency from 0.01 to 100 Hz, the storage modulus drastically changed from 0.29 to 34.2 MPa, corresponding to a 117-fold increase in stiffness. Notably, the lower modulus of 0.29 MPa still meets the Dahlquist criterion for effective tackiness (<0.3 MPa).^[15] The relaxation spectrum was additionally generated from the rheological master curve, which clearly discerned two relaxation modes in the ionogel (Figure 3f).^[39] We ascribed the peak at the lower relaxation time to the more mobile and strongly ionophilic P[DMAEA-Q-TFSI] moieties, while the other peak at the higher relaxation time to the less mobile and weakly ionophilic PDMA moieties. Their distinct relaxations at different timescales serve as the basis for peeling-induced phase separation, which will be discussed later.

To further demonstrate the frequency-dependent dissipatingto-glassy transition, we investigated the tensile behavior of the ionogel at different strain rates. As shown in Figure 3g, at the very low strain rate of 0.002 s⁻¹, the ionogel plastically deformed with strain softening, resulting in an ultrahigh elongation of 3215% and a low Young's modulus of 3.7 MPa. However, increasing the strain rate to 0.02, 0.1, and 0.5 s⁻¹ led to significantly increased Young's moduli of 18.3, 40.1, and 61.6 MPa, respectively. The appearance of pronounced yielding revealed that the ionogel had transformed into a glassy state at high strain rates. In accordance with the Eyring model, [40] we calculated the activation volume and energy to be 11.5 nm³ and 12.6 kJ mol⁻¹, respectively, which can be interpreted as the segmental size and energy barrier for the dissociation of noncovalent bonds under force in yielding (Figure 3h). Moreover, with increasing strain rates, the mechanical response transformed from strain softening to strain hardening, suggesting the formation of stronger physical cross-links (i.e., PDMA-rich nanophases) at high strain rates.[41]

As mentioned, the frequency-dependent dissipating-to-glassy transition of the self-adhesive ionogel led to the unusual peelingstiffening response in adhesion. To prove this, we tested the interfacial toughness of the ionogel at different peeling speeds (Figure 3i,j). With increasing peeling speed from 1 to 50 mm min⁻¹, the interfacial toughness significantly increased from 872 \pm 164 to 8046 \pm 582 J m⁻². This arises from the transition from a dissipating state at a low peeling speed of 1 mm min⁻¹ (corresponding to ≈ 0.33 Hz, $G' \approx 4.7$ MPa) to the glassy state at the high peeling speeds of 10 mm min⁻¹ (corresponding to ≈ 3.3 Hz, $G' \approx 16.6$ MPa) and 50 mm min⁻¹ (corresponding to 16.7 Hz, $G' \approx 24.7 \text{ MPa}$). Finite element simulation results further supported the above conclusion (Figure S17 and Movie S4, Supporting Information). The sensitivity in this range was calculated to be 146.4 J m⁻² per mm min⁻¹, much higher than those of commercial VHB tape (5.2 J m⁻² per mm min⁻¹, Figure S18, Supporting Information) and other reported adhesive materials (e.g., polyacrylamide/alginate hydrogel on glass, 10.6 J m⁻² per mm min⁻¹; topological adhesion of hydrogels, 4.3 J m⁻² per mm min⁻¹).[10,42] However, further increasing the peeling speed to 150 and 300 mm min⁻¹ caused the interfacial toughness to decline. This trend is consistent with the changes in fracture energy, which also culminated at a moderate strain rate (0.1 s⁻¹, Figures S19,S20, Supporting Information). It is understandable that the fracture energy and interfacial toughness of the supramolecular ionogel will eventually be reduced when more and more polymer chains are frozen at high strain rates and cannot effectively dissipate strain energy.

2.3. Mechanism Discussion for Peeling-Stiffening Response

It is the key to interpreting the peeling-stiffening response at the nanostructure and molecular levels to account for the strong adhesion of the present self-adhesive ionogel. As illustrated in Figure 4a, we ascribed the peeling-stiffening response to the strain-rate-induced spontaneous formation of aligned nanophases (or hard domains), which not only enhances physical cross-linking density for stiffening but also blunts the cracks to inhibit interfacial failure. The occurrence of nanophase separation can be directly observed from its color changes. Upon stretch to 400% at the constant strain rate of 0.1 s⁻¹, the ionogel gradually changed from transparent to light blue (Movie S5, Supporting Information), indicating the formation of nanophases that started to scatter visible light.^[43] Similar phenomenon can also be observed when we stretched the sample to a fixed strain of 400% at increasing strain rates (Figure S21, Supporting Information). Atomic force microscopy (AFM) observations confirmed the growth of aligned nanophases along the stretching direction (Figure 4b). Small-angle X-ray scattering (SAXS) results indicated that the system exhibited a loose matrix structure at 0% strain (Figure 4c). However, stretching led to the collapse of the matrix structure, resulting in the emergence of new, densely packed nanophases with dimensions larger than 100 nm. This transformation was also supported by a significant increase in intensity and a shift in the power law scattering exponent from -2.3 at 0% strain to -3.5 at 400% strain within the low q regime. According to our findings in fracture-tolerant hydrogel microfiber, the formed hard nanophases as geometric nanoconfinement can greatly enlarge the crack process zone size and thus increase the energy to fracture the material.^[41] Indeed, when we stretched a notched ionogel, the introduced crack did not apparently propagate along with phase separation (Figure S22, Supporting Information). Notably, the enhancement of interfacial adhesion by phase separation has also been recently observed in several other adhesive materials.[7,19,25,26]

To gain molecular insights into the nanostructure changes of the ionogel, we collected the temperature-dependent 1D/2D lowfield ¹H NMR and IR spectra. Low-field ¹H NMR is a powerful tool to monitor the activity changes of hydrogen atoms via spin–spin relaxation time (T_2) . [44] At temperatures lower than T_g (23 °C), only one T_2 peak was observed, suggesting the cooperative motions of all the moieties in the ionogel (Figure 4d). Further increasing the temperature distinguished three species with increasing relaxation times, which can be assigned to PDMA, P[DMAEA-Q-TFSI], and EMI ES, respectively. The motion of PDMA lagged behind those of P[DMAEA-Q-TFSI] and EMI ES, suggesting its lower activity. The three species can also be clearly observed in the corresponding 2D T_1 – T_2 plot (T_1 : spin–lattice relaxation time) at 125 °C (Figure 4e), which is a measure of molecular mobilities. Generally, a lower T_1/T_2 ratio means a higher mobility (the diagonal line with equal T_1 and T_2 denotes a completely

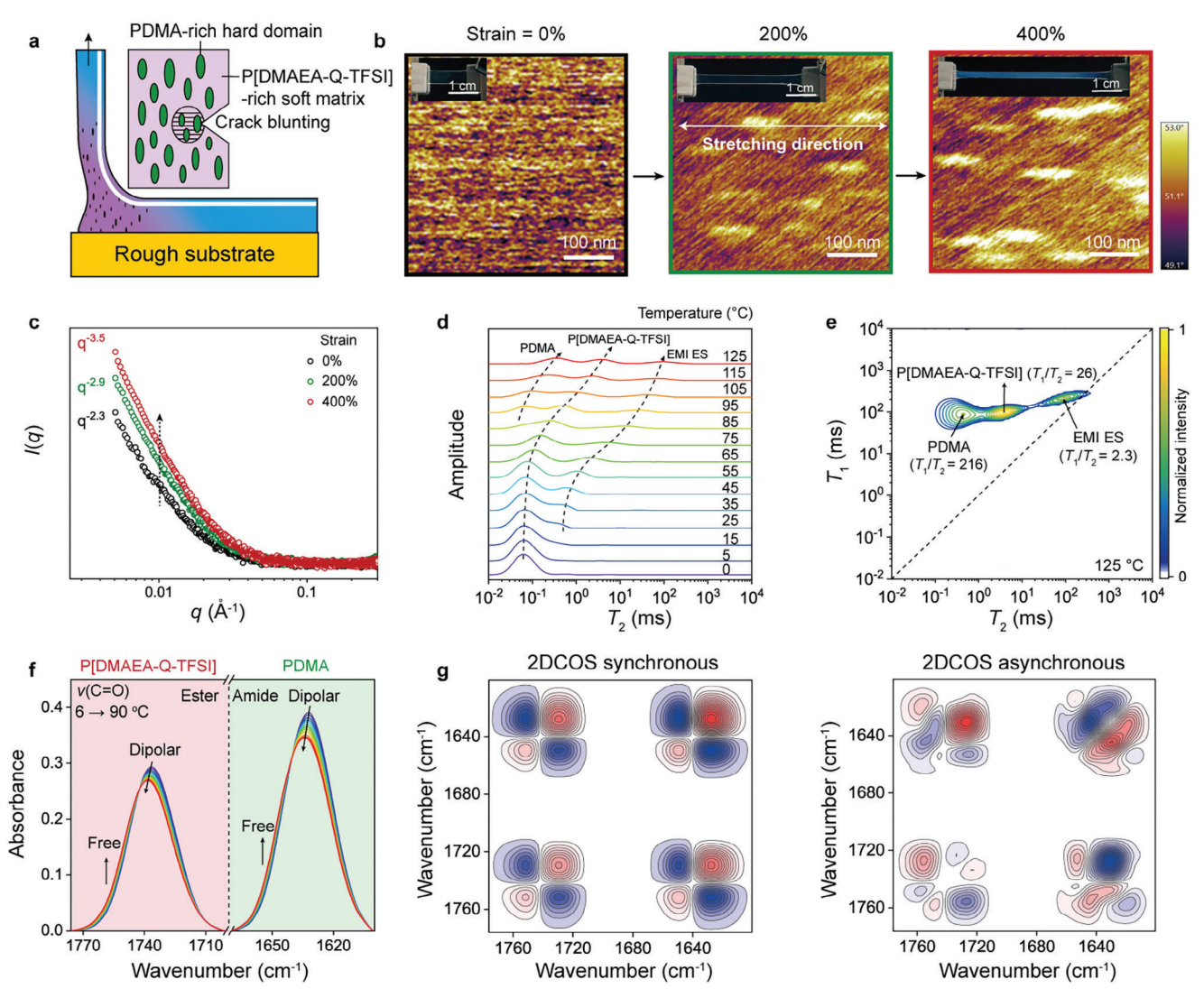


Figure 4. a) Proposed mechanism for the peeling–stiffening response of the self-adhesive ionogel. Upon peeling, the self-aggregation of PDMA moieties takes place, forming hard nanodomains that enhance physical cross-linking and inhibit crack propagation. b) Photos and AFM phase images of the ionogel as stretched to 200% and 400% strains at the strain rate of $0.1 \, \text{s}^{-1}$. c) SAXS curves of the ionogel as stretched to different strains. The scattered intensities were rescaled by the high q data for comparison. d) Temperature-variable low-field 1 H NMR spectra. e) 2D low-field 1 H NMR spectrum of the ionogel at 125 °C. f) Temperature-dependent FTIR spectra and the corresponding assignments (interval: 8 °C). g) 2DCOS synchronous and asynchronous spectra generated from (f). The red colors represent positive intensities, while the blue colors represent negative intensities.

mobile liquid state). The cross-peak for PDMA has a very high T_1/T_2 ratio of 216, significantly higher than that for P[DMAEA-Q-TFSI] (T_1/T_2 = 26) and EMI ES (T_1/T_2 = 2.3). This reveals that in the ionogel, PDMA moieties with the lowest mobility are inclined to self-aggregate to form a separated phase with the matrix of P[DMAEA-Q-TFSI]/EMI ES.

The internal interactions in the ionogel were studied in detail by 1D/2D IR spectroscopy. Attenuated total reflection Fourier-transform infrared (ATR-FTIR) spectral comparison showed that, upon introducing EMI ES, EMI cations mainly bound to the ester C=O groups of P[DMAEA-Q-TFSI] via ion—dipole interactions, and ES anions exchanged with TFSI, resulting in the shifts of all related vibrations (Figure S23, Supporting Information). By contrast, the amide C=O stretching vibration of PDMA did not significantly change with introducing EMI ES, suggesting the weak

interactions between them. These results support the above conclusion about the lower mobility of PDMA moieties in the ionogel. To elucidate the sensitivities of different moieties, we then collected the temperature-variable transmission IR spectra of the ionogel in the C=O stretching region from 6 to 90 °C (Figure 4f). Obviously, heat weakened all the internal interactions, causing both the shifts of dipolar ν (C=O) (P[DMAEA-Q-TFSI]) and dipolar ν (C=O) (PDMA) to higher wavenumbers, as well as the emergence of free ν (C=O) signals.

2D correlation spectra (2DCOS) were further generated from all the temperature-variable IR spectra to extract more subtle information about sequential events during heating (Figure 4g). [45,46] Following Noda's judging rule based on the signs of cross-peaks in the synchronous and asynchronous spectra, the sequential order of C=O related species upon

heating was determined to be (→ indicates prior to or earlier than; see Table S2, Supporting Information for determination details): $1645 \rightarrow 1728 \rightarrow 1734 \rightarrow 1616 \rightarrow 1749 \rightarrow 1653$ \rightarrow 1755 \rightarrow 1630 cm⁻¹, i.e., ν (C=O) (PDMA...EMI) \rightarrow ν (C=O) (P[DMAEA-Q-TFSI], strongly dipolar) $\rightarrow \nu$ (C=O) (P[DMAEA-Q-TFSI], weakly dipolar) $\rightarrow \nu$ (C=O) (PDMA, strongly dipolar) \rightarrow ν (C=O) (P[DMAEA-Q-TFSI]...EMI) $\rightarrow \nu$ (C=O) (PDMA, free) \rightarrow ν (C=O) (P[DMAEA-Q-TFSI], free) $\rightarrow \nu$ (C=O) (PDMA, weakly dipolar). 2DCOS greatly enhanced spectral resolution by discerning each four conformations of v(C=O) for PDMA and P[DMAEA-Q-TFSI], respectively. EMI cations can interact with both the ester groups of P[DMAEA-Q-TFSI] and amide groups of PDMA, which accounts for their compatibilities with EMI ES. Importantly, PDMA moieties associated with EMI are most susceptible to environmental changes with the earliest response upon heating. This explains that upon stretch, PDMA moieties are inclined to self-aggregate into hard nanophases, which are the driving force for phase separation. The self-aggregation of PDMA moieties was additionally supported by monitoring the ν (C=O) peak of amide groups upon stretch, which shifted to lower wavenumbers corresponding to stronger dipolar interactions (Figure S24, Supporting Information).

Based on the above analyses, we conclude that the peeling-stiffening response of the self-adhesive ionogel should arise from the strain-rate-induced phase separation of PDMA moieties, which form numerous hard nanophases that greatly enhance physical cross-linking and inhibit crack propagation. The key design of the copolymer ionogel lies on the subtle balance of the compatibility between PDMA moieties and the soft matrix of P[DMAEA-Q-TFSI]/EMI ES. That is, at the initial quasistatic state, PDMA moieties are compatible with the P[DMAEA-Q-TFSI]/EMI ES matrix, resulting in a homogeneous structure locating in the liquid-like dissipating region. However, upon stretching/peeling, the compatibility balance is disrupted, leading to the self-aggregation of PDMA moieties and final phase separation.

To emphasize the copolymer design in attaining strong adhesion, we also prepared PDMA/EMI ES and P[DMAEA-Q-TFSI]/EMI ES homopolymer ionogels as controls. We carefully adjusted the EMI ES content to 55 wt% for PDMA and 5 wt% for P[DMAEA-Q-TFSI], respectively, to make their $T_{\rm g}$ s also close to room temperature (i.e., working in the dissipating state). However, the calculated fracture energies and interfacial toughnesses of two homopolymer ionogels are much lower than the copolymer ionogel (Figures S25,S26, Supporting Information).

2.4. Self-Healing, Recycling, Detaching, and Impact-Protecting Properties

The supramolecular nature also imparts self-healing, recycling, and on-demand detaching properties to the self-adhesive ionogel, which are important for its sustainable uses. We demonstrated the self-healing property by adhering two ionogel samples at 50 °C for 6 h, and the resulting adhered ionogel was not only stretchable, but also easily sustained a 1 kg weight load (**Figure 5a**). The healing efficiency was $\approx 96\%$ as evaluated by the fracture strength and maximum elongation (Figure 5b). The ionogel can also be readily dissolved in acetonitrile within 30 min,

and recast into a new film after solvent evaporation (Figure 5c). The recast ionogel still exhibited an exceptional interfacial toughness of up to 6188 J m $^{-2}$ (Figure 5d). We ascribed the slightly lower adhesion of the recast ionogel than the original one to the loss of effective chain entanglement in the evaporation process compared to the in situ polymerized network.

There is always a trade-off between strong adhesion and easy detachment for conventional adhesives. [3,4,47] After peeling, the residues of strong adhesive materials may also present a predicament for the recycling of substrate materials. By contrast, owing to the hydrophilicity of EMI ES and PDMA moieties, the strong adhesion of the ionogel can be easily removed by simple moisture treatment. The permeable water molecules not only induced apparent phase separation (from transparent to opaque) but also the significant degradation of mechanical properties of the ionogel (Figure S27, Supporting Information). Moreover, water molecules would migrate to the adhering interface as the lubricant and thus destroy the mechanical interlocking state. As a result, the measured interfacial toughness of the ionogel after treating with high relative humidity (RH 90%) for 12 h decreased dramatically to only 136 J m⁻² (Figure 5e). The bonding/debonding ratio is 59, surpassing most reversible adhesives (Figure 5f and Table S3 (Supporting Information)). Directly immersing the adherend with the ionogel in water would even accelerate this debonding process in merely 30 min (Figure S28, Supporting Information).

The present self-adhesive ionogel with integrated superstrong adhesion and ionic conductivity may gain promising applications in diverse fields ranging from packaging and coating to soft electronics, soft machines, and soft actuators. [1,10,30,48] Considering its potential contact with human body, we also evaluated the ionogel's biocompatibility by cytotoxicity tests on HeLa cells, which exhibited remarkably high cell viability even after 48 h (Figure \$29, Supporting Information). Here, we demonstrated a typical application of the self-adhesive ionogel in simultaneous impact protection and sensing. Laminated glass is a type of safety glass that prevents the glass from breaking into large, sharp pieces. It is widely used in windows, automobile windshields, skylight glazing, and other applications. Conventional laminated glass consists of two or more plies of glass bonded with polymer interlayers, such as polyvinyl butyral and ethylene-vinyl acetate. Here, we prepared a smart laminated glass by bonding two plies of glass using our ionogel, which has both strong self-adhesion and ionic conductivity (conductivity $\approx 8.3 \times 10^{-6} \text{ S m}^{-1}$, Figure S30, Supporting Information). As shown in Figure 5g, owing to the high transparency of the ionogel, the obtained laminated glass remained highly transparent with a transparency of \approx 80%. The strong adhesion and energy-dissipating properties of the ionogel endowed the laminated glass with excellent impact-protecting properties. As depicted in the impact test, the ionogel-bonded laminated glass can withstand an impact force up to 8000 N, while the control ordinary glass without ionogel fractured at only 2500 N (Figure 5h). After impact, the ionogel-bonded laminated glass retained its structural integrity with a characteristic "spider web" cracking pattern, in stark contrast to the ordinary glass, which shattered into fragments (Figure 5i and Movie S6 (Supporting Information)).

Moreover, the ionically conductive ionogel interlayer can also serve as the triboelectric electrode for self-powered impact

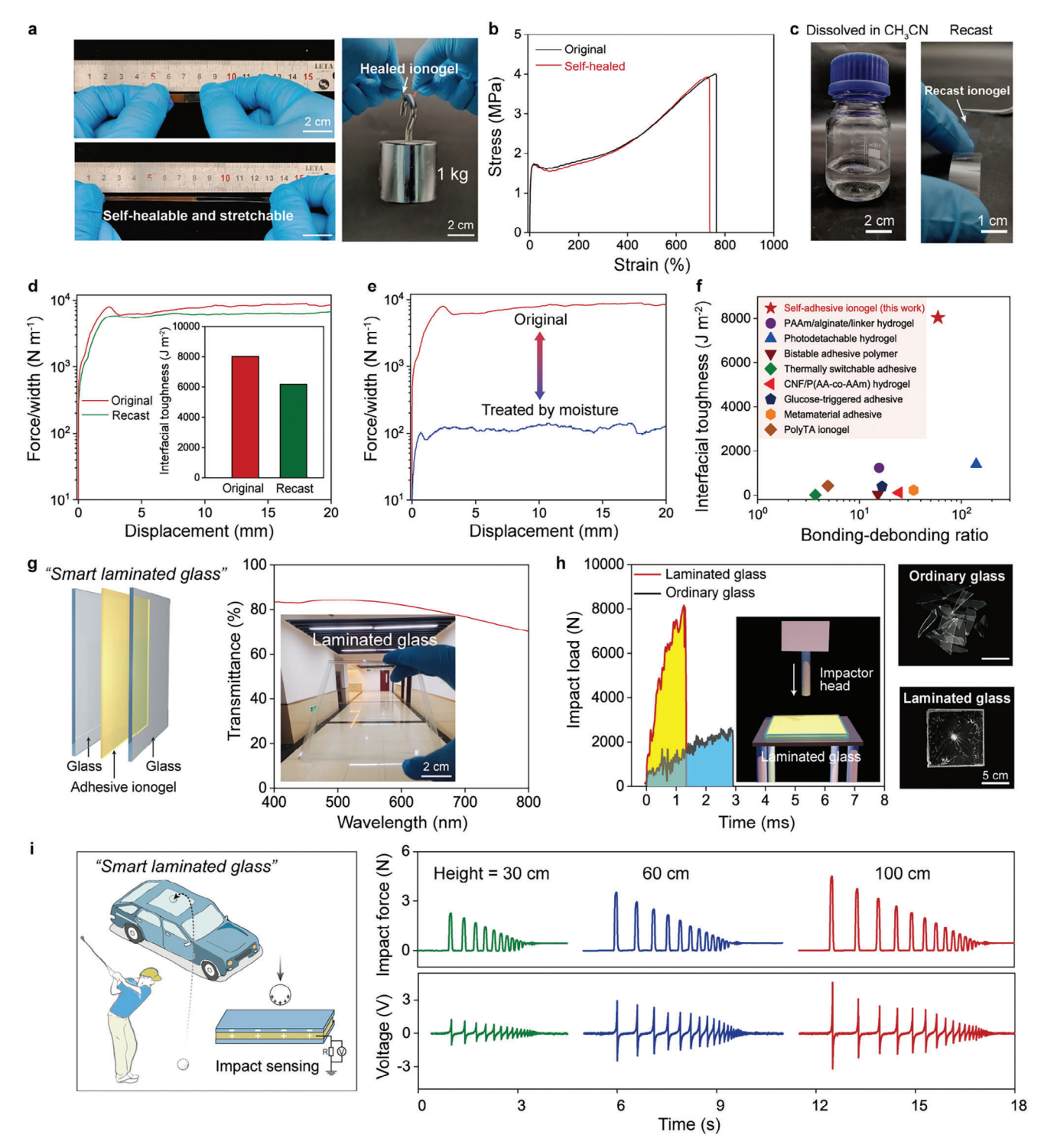


Figure 5. a) The healed self-adhesive ionogel is stretchable and sustains a 1 kg weight load. b) Tensile curves of the original and self-healed ionogels. c) The ionogel can be dissolved in acetonitrile and recast into a new film. d) Interfacial toughnesses of the original and recast ionogels. e) Interfacial toughnesses of the ionogels before and after moisture treatment at RH 90% for 12 h. f) Comparison of interfacial toughnessess and bonding—debonding ratios among typical reversible adhesive materials (data in Table S3 in the Supporting Information). g) Schematic construction and transmittance of the ionogel-bonded smart laminated glass (the thicknesses of glass and ionogel are 3 and 1 mm, respectively). h) Time-resolved impact load curves and photos of laminated and ordinary glasses. i) Triboelectric impact sensing by falling a golf ball from different heights.

sensing (Figure S31, Supporting Information).^[49] Initial tests have shown that the laminated glass can respond to diverse contact materials and different pressures with real-time voltage changes (Figure S32, Supporting Information). Additionally, we simulated a real scenario by impacting an automobile skylight window with a golf ball. As shown in Figure 5j, a series of oscillating voltage signals were recorded after dropping the golf ball from different heights on the smart laminated glass, which can directly reflect the changes in impact forces.

3. Conclusion

In this paper, we propose a new concept of peeling-stiffening self-adhesive materials, in contrast to conventional cured and pressure-sensitive adhesives. Peeling-stiffening self-adhesive materials utilize a frequency-dependent dissipating-to-glassy transition that reconciles the long-term trade-off between intrinsic softness and strong adhesion in self-adhesive materials. To prove this concept, we designed a supramolecular copolymer ionogel consisting of two ionophilic repeating units with different associating affinities to the ionic liquid. At the initial quasistatic state, the optimized copolymer ionogel works in the liquid-like dissipating region, enabling excellent interfacial adaptability for adhesion. However, upon peeling at higher frequencies, the ionogel rapidly stiffens to the glassy state with a 117-fold increase in stiffness. This peeling-stiffening response is driven by the strain-rate-induced phase separation of PDMA moieties, which greatly suppresses crack propagation and leads to a superhigh interfacial toughness of 8046 \pm 582 J m⁻². Additionally, the dynamic nature of the ionogel endows it with high transparency, stretchability, self-healability, recyclability, and easy detachment. The application of the self-adhesive ionogel in smart laminated glass demonstrates its great potential in simultaneous impact protection and sensing. We anticipate that the peeling-stiffening concept will be extended to design other highperformance self-adhesive materials for intelligent soft electronics and robotics.

Supporting Information

Supporting Information is available from the Wiley Online Library or from the author.

Acknowledgements

The authors appreciate the support from the National Natural Science Foundation of China (NSFC) (Grant Nos. 52322306, 21991123, 52161135102, 22275032, 51973035). S.T.S. thanks the supports from Shanghai Oriental Talent Program and Talent Development Fund. The authors also thank Dr. Lingyan Liu of the Donghua University for the assistance in cytotoxicity test.

Conflict of Interest

The authors declare no conflict of interest.

Data Availability Statement

The data that support the findings of this study are available from the corresponding author upon reasonable request.

Keywords

adhesives, impact protection, ionogels, phase separation, responsive materials

- [1] J. Yang, R. Bai, B. Chen, Z. Suo, Adv. Funct. Mater. 2020, 30, 1901693.
- [2] Y. Zhao, S. Song, X. Ren, J. Zhang, Q. Lin, Y. Zhao, Chem. Rev. 2022, 122, 5604.
- [3] D. Hwang, C. Lee, X. Yang, J. M. Pérez-González, J. Finnegan, B. Lee, E. J. Markvicka, R. Long, M. D. Bartlett, Nat. Mater. 2023, 22, 1030.
- [4] C. Linghu, Y. Liu, Y. Y. Tan, J. H. M. Sing, Y. Tang, A. Zhou, X. Wang, D. Li, H. Gao, K. J. Hsia, *Proc. Natl. Acad. Sci. USA* 2023, 120, 2221049120.
- [5] A. Tiwari, J. Wang, B. N. J. Persson, Phys. Rev. E 2020, 102, 042803.
- [6] K. Kendall, Molecular Adhesion and Its Applications: The Sticky Universe, Springer, New York 2001.
- [7] J. Liu, S. Lin, X. Liu, Z. Qin, Y. Yang, J. Zang, X. Zhao, Nat. Commun. 2020, 11, 1071.
- [8] L. Liu, Z. Liu, Y. Ren, X. Zou, W. Peng, W. Li, Y. Wu, S. Zheng, X. Wang, F. Yan, Angew. Chem., Int. Ed. 2021, 60, 8948.
- [9] S. Xi, F. Tian, G. Wei, X. He, Y. Shang, Y. Ju, W. Li, Q. Lu, Q. Wang, Adv. Mater. 2021, 33, 2103174.
- [10] H. Yuk, T. Zhang, S. Lin, G. A. Parada, X. Zhao, Nat. Mater. 2016, 15, 190.
- [11] S. Choi, J. R. Moon, N. Park, J. Im, Y. E. Kim, J.-H. Kim, J. Kim, Adv. Mater. 2023, 35, 2206207.
- [12] M. Guo, G. Li, M. Cai, X. Hou, K. Huang, J. Tang, C. F. Guo, Nano Lett. 2023, 23, 1371.
- [13] Y. Yu, H. Yuk, G. A. Parada, Y. Wu, X. Liu, C. S. Nabzdyk, K. Youcef-Toumi, J. Zang, X. Zhao, Adv. Mater. 2019, 31, 1807101.
- [14] H. Cho, G. Wu, J. Christopher Jolly, N. Fortoul, Z. He, Y. Gao, A. Jagota, S. Yang, Proc. Natl. Acad. Sci. USA 2019, 116, 13774.
- [15] E. P. Chang, J. Adhes. 1991, 34, 189.
- [16] E. Arzt, H. Quan, R. M. Mcmeeking, R. Hensel, Prog. Mater. Sci. 2021, 120, 100823.
- [17] K. Li, X. Zan, C. Tang, Z. Liu, J. Fan, G. Qin, J. Yang, W. Cui, L. Zhu, Q. Chen, Adv. Sci. 2022, 9, 2105742.
- [18] W. Niu, J. Zhu, W. Zhang, X. Liu, ACS Mater. Lett. 2022, 4, 410.
- [19] T. Nogusa, C. B. Cooper, Z. Yu, Y. Zheng, Y. Shi, Z. Bao, *Matter* **2023**, 6. 2439.
- [20] Z. Yu, P. Wu, Adv. Mater. 2021, 33, 2008479.
- [21] C. Xie, X. Wang, H. He, Y. Ding, X. Lu, Adv. Funct. Mater. 2020, 30, 1909954.
- [22] J. Huang, Y. Liu, Y. Yang, Z. Zhou, J. Mao, T. Wu, J. Liu, Q. Cai, C. Peng, Y. Xu, B. Zeng, W. Luo, G. Chen, C. Yuan, L. Dai, Sci. Rob. 2021, 6, eabe 1858.
- [23] Y. Miao, M. Xu, L. Zhang, Adv. Mater. 2021, 33, 2102308.
- [24] Y. Zhang, S. Zhang, F. Sun, Q. Ji, J. Xu, B. Yao, Z. Sun, T. Liu, G. Hao, Y. Hu, G. Zhang, W. Jiang, J. Fu, Adv. Funct. Mater. 2023, 33, 2304653.
- [25] M. Li, H. Lu, M. Pi, H. Zhou, Y. Wang, B. Yan, W. Cui, R. Ran, Adv. Sci. 2023, 10, 2304780.
- [26] W. Cui, R. Zhu, Y. Zheng, Q. Mu, M. Pi, Q. Chen, R. Ran, J. Mater. Chem. A 2021, 9, 9706.
- [27] H. Yuk, T. Zhang, G. A. Parada, X. Liu, X. Zhao, Nat. Commun. 2016, 7, 12028.
- [28] Z. Pan, Q.-Q. Fu, M.-H. Wang, H.-L. Gao, L. Dong, P. Zhou, D.-D. Cheng, Y. Chen, D.-H. Zou, J.-C. He, X. Feng, S.-H. Yu, *Nat. Commun.* 2023, 14, 5378.

- [29] A. Inoue, H. Yuk, B. Lu, X. Zhao, Sci. Adv. 2020, 6, eaay5394.
- [30] D. Wirthl, R. Pichler, M. Drack, G. Kettlguber, R. Moser, R. Gerstmayr, F. Hartmann, E. Bradt, R. Kaltseis, C. M. Siket, S. E. Schausberger, S. Hild, S. Bauer, M. Kaltenbrunner, Sci. Adv. 2017, 3, 1700053.
- [31] Y.-J. Wang, Y. He, S. Y. Zheng, Z. Xu, J. Li, Y. Zhao, L. Chen, W. Liu, Adv. Funct. Mater. 2021, 31, 2104296.
- [32] M. J. Webber, M. W. Tibbitt, Nat. Rev. Mater. 2022, 7, 541.
- [33] C. Creton, M. Ciccotti, Rep. Prog. Phys. 2016, 79, 046601.
- [34] B. Liu, T. Yin, J. Zhu, D. Zhao, H. Yu, S. Qu, W. Yang, Proc. Natl. Acad. Sci. USA 2023, 120, 2217781120.
- [35] H. Xiang, X. Li, B. Wu, S. Sun, P. Wu, Adv. Mater. 2023, 35, 2209581.
- [36] J. Zhang, Z. Chen, Y. Zhang, S. Dong, Y. Chen, S. Zhang, Adv. Mater. 2021, 33, 2100962.
- [37] J. Zhang, W. Wang, Y. Zhang, Q. Wei, F. Han, S. Dong, D. Liu, S. Zhang, Nat. Commun. 2022, 13, 5214.
- [38] W. Peng, G. Zhang, Q. Zhao, T. Xie, Adv. Mater. 2021, 33, 2102473.

- [39] S. C. Grindy, R. Learsch, D. Mozhdehi, J. Cheng, D. G. Barrett, Z. Guan, P. B. Messersmith, N. Holten-Andersen, *Nat. Mater.* 2015, 14, 1210.
- [40] C. Bilici, S. Ide, O. Okay, Macromolecules 2017, 50, 3647.
- [41] Y. Shi, B. Wu, S. Sun, P. Wu, Nat. Commun. 2023, 14, 1370.
- [42] J. Yang, R. Bai, Z. Suo, Adv. Mater. 2018, 30, 1800671.
- [43] M. Yao, B. Wu, X. Feng, S. Sun, P. Wu, Adv. Mater. 2021, 33, 2103755.
- [44] Y.-Q. Song, R. Kausik, Prog. Nucl. Magn. Reson. Spectrosc. 2019, 112– 113, 17.
- [45] W. Zhang, B. Wu, S. Sun, P. Wu, Nat. Commun. 2021, 12, 4082.
- [46] S.-T. Sun, P.-Y. Wu, Chin. J. Polym. Sci. 2017, 35, 700.
- [47] W. Li, X. Liu, Z. Deng, Y. Chen, Q. Yu, W. Tang, T. L. Sun, Y. S. Zhang, K. Yue, Adv. Mater. 2019, 31, 1904732.
- [48] Y. Wang, S. Sun, P. Wu, Adv. Funct. Mater. 2021, 31, 2101494.
- [49] H. Qiao, S. Sun, P. Wu, Adv. Mater. 2023, 35, 2300593.